Advanced Design of a Transition Duct for Supersonic Inlet Turbines in Rotating Detonation Engines

Mushtaq, Noraiz; Pini, Matteo; Gaetani, Paolo

DOI
10.1115/1.4067242

Publication date
2025

Document Version
Final published version

Published in
Journal of Turbomachinery

Citation (APA)
Mushtaq, N., Pini, M., & Gaetani, P. (2025). Advanced Design of a Transition Duct for Supersonic Inlet Turbines in Rotating Detonation Engines. *Journal of Turbomachinery*, *147*(3), Article 031014. https://doi.org/10.1115/1.4067242

ASME Journal of Turbomachinery
Online journal at:
https://asmedigitalcollection.asme.org/turbomachinery

Advanced Design of a Transition Duct for Supersonic Inlet Turbines in Rotating Detonation Engines

Noraiz Mushtaq
Laboratory of Fluid Machines (LFM),
Politecnico di Milano,
Via Lambruschini 4,
Milan 20156, Italy
e-mail: noraiz.mushtaq@polimi.it

Matteo Pini
Propulsion and Power,
Faculty of Aerospace Engineering,
Delft University of Technology,
Kluyverweg 1,
Delft 2629 HS, The Netherlands
e-mail: m.pini@tudelft.nl

Paolo Gaetani[1]
Laboratory of Fluid Machines (LFM),
Politecnico di Milano,
Via Lambruschini 4,
Milan 20156, Italy
e-mail: paolo.gaetani@polimi.it

A supersonic inlet turbine can extract substantial energy from the highly fluctuating and transonic flow delivered by a rotating detonation combustor (RDC). However, a transition duct is necessary to achieve the supersonic inlet conditions required by the turbine. In this work, the supersonic transition duct is designed with the method of characteristics (MOC). A generalized implementation of the MOC is proposed for the generation of annular ducts with asymmetric and rotated hub and shroud walls. The model is extended to deal with ideal and non-ideal flows, namely flows characterized by non-ideal thermodynamic effects, and its accuracy has been verified through comparison with results obtained with computational fluid dynamics (CFD) simulations. In addition, boundary layer flow equations are combined with the MOC to predict viscous losses on the endwalls and to adjust duct geometry by accounting for the boundary layer thickness. Furthermore, it is essential to predict the effects of the large unsteadiness generated by the detonation combustor for an efficient operation of the turbine. The maximum incidence angle at the turbine inlet is predicted with a one-dimensional annular duct model. Supersonic duct flow behavior to unsteady inlet conditions is characterized through two-dimensional inviscid axisymmetric unsteady CFD simulations. The accuracy of the reduced order models is finally verified with a three-dimensional unsteady viscous simulation assuming inlet flow conditions representative of RDC operation. [DOI: 10.1115/1.4067242]

Keywords: rotating detonation engine, supersonic transition duct, method of characteristics, reduced-order models

1 Introduction

A detonation wave rotates and burns the fresh mixture injected in a rotating detonation combustor (RDC) [1]. The rotating detonation engine (RDE), a gas turbine integrated with the RDC, offers several advantages, including reduced fuel consumption [2,3], a rise in total pressure [4], and increased thermal plant efficiency [5]. Moreover, the operational flexibility of RDEs and their compatibility with various fuels, including hydrogen [6], emphasize their potential in the evolving energy landscape of the coming decades, which anticipates a substantial integration of renewable but non-schedulable technologies into the overall energy mix [7]. Anand and Gutmark [6], Ma et al. [8], and Raman et al. [9] have provided a comprehensive overview of the challenges surrounding the physics of RDCs, shedding light on the complexity of this innovative technology.

The flow delivered by an RDC is transonic and highly fluctuating [10]. These flow conditions are critical when integrating the combustion chamber with a subsonic or a supersonic turbine. In a subsonic turbine, the flow turning is notably limited due to choking at high subsonic inlet Mach numbers [11]. Meanwhile, the design of a supersonic turbine is constrained by Kantrowitz unstarting [12], collective shock unstarting [13], and unique incidence [14], where the severity of each of these constraints is more pronounced at low supersonic inlet Mach numbers. Hence, the architecture of an RDE necessitates a diffusing or accelerating transition duct to couple the RDC with the high-pressure turbine. This work focuses on the supersonic configuration of a rotating detonation engine.

The mean-line design of supersonic axial inlet turbines for RDEs has been detailed by Paniagua et al. [15] and by Mushtaq et al. [16]. Inhestern et al. [17] have presented the alternative option of a supersonic radial outflow turbine to exploit the natural increase of cross section along the flow path. Various optimization procedures have been developed to improve the different elements of a supersonic turbine: Sousa and Paniagua [18] optimized the profile of the supersonic blade, while Mushtaq et al. proposed methodologies for cascade solidity [16] and endwall shape optimization [19]. Sousa et al. [20] examined the performance of supersonic passages when operating with pulsating inlet conditions, while Mushtaq and Gaetani [21] investigated the effect of upstream unsteadiness on the unstarting phenomena of these machines. Supersonic turbine interaction with the RDC has been investigated numerically by Sousa et al. [20], Braun et al. [22], Shen et al. [23], and Su et al. [24], and experimentally by Bach et al. [25].

Over the past decade, various accelerating or diffusing transition duct designs have been evaluated for RDE-based applications. Braun et al. explored five different nozzle shapes and compared their performance in terms of pressure gain loss [26]. Their findings

[1]Corresponding author.

Contributed by International Gas Turbine Institute (IGTI) of ASME for publication in the Journal of Turbomachinery. Manuscript received September 2, 2024; final manuscript received November 11, 2024; published online December 17, 2024. Tech. Editor: David G. Bogard.

indicate that for supersonic flows smooth diverging nozzles are the most effective in attenuating the fluctuations with a reasonable increase in flow momentum [27], and the total pressure losses of an accelerating passage are almost half compared to a diffusing passage [28]. Experiments by Nakata et al. [29,30] demonstrate that a supersonic flow condition can be achieved without a geometrically converging section because thermal choking is almost instantaneously achieved thanks to the huge amount of heat released by the detonation combustion. Furthermore, Sun et al. [31] observed that outlet nozzles could influence wave collisions within the combustor, but the fundamental propagation process remained similar to the case without the nozzle.

Most research on the transition duct has approached the problem from an analysis point of view: the focus of the researchers was the aerodynamic study of the flow in the channel, while simple and non-optimal strategies were adopted for the design of the nozzle. The proper design of the duct can therefore lead to improved performance of the engine. Designing supersonic transition ducts requires however ad hoc methods for treating unsteady supersonic flows. To this end, the availability of reduced-order models for predicting and mitigating the impact of unsteadiness and viscous dissipation on performance at low cost is crucial. This work aims to fill the existing knowledge gap in the literature by proposing a novel design methodology for supersonic transition ducts. The developed methodology encompasses computationally efficient reduced-order models, whose accuracy is verified against the results of unsteady Reynolds-averaged Navier–Stokes.

The structure of this paper is as follows. Section 2 describes the computational flow model employed for the various computational fluid dynamics (CFD) simulations carried out throughout this work. A generalized formulation of the method of characteristics for rotated annular asymmetric ducts is presented in Sec. 3. The methodology is developed to accommodate fluids with properties defined by an arbitrary equation of state model. The method to compute viscous dissipation is documented in Sec. 4. A one-dimensional annular duct model to estimate the amplitude of the outlet flow angle fluctuations is presented in Sec. 5. Moreover, Sec. 5 reports on the results of the study of the response of the supersonic channel to unsteady inlet conditions, performed with two-dimensional inviscid axisymmetric unsteady CFD simulations. Results obtained with three-dimensional unsteady viscous simulation of the flow within the transition duct assuming inlet conditions representative of RDC engines are finally illustrated.

2 Computational Flow Model

The flow in the transition duct was studied with axisymmetric two-dimensional and three-dimensional computational fluid dynamic simulations. All the computations were carried out with the implicit pressure-based coupled solver of ANSYS FLUENT [32]. The advection terms were discretized with the QUICK scheme [33], and a second-order bounded implicit integration was employed for temporal discretization. Gradients were determined with the least squares cell-based method, and the pressure was interpolated on the faces with a second-order scheme. For the viscous simulations, turbulence closure was achieved with the $k-\omega$ shear stress transport model [34], ensuring that y^+ was maintained below 1 for accurate boundary layer resolution on the walls.

Total pressure, total temperature, and static pressure (this last input is considered by the solver only for supersonic inlet conditions) were assigned at the inlet. At the outlet, only the static pressure was specified. Adiabatic free-slip and no-slip boundary conditions were set on the hub and shroud walls for inviscid and viscous simulations. The computational costs of the 3D simulation (Sec. 5) were mitigated by considering a 90 deg tangential extension of the domain complemented with periodic boundary conditions on the lateral faces.

Convergence was achieved when the residuals were below 10^{-6} at each time-step (or the final step for a steady-state simulation). Unsteady simulations with periodic inlet conditions were discretized with 240 time-steps per period: the number of steps was selected to accurately reproduce the profile in time of the inlet conditions and to capture all relevant frequencies according to the Whittaker–Shannon sampling theorem [35]. Periodic convergence was evaluated with Clark's methodology [36]. The selected fuzzy sets compare consecutive periods in terms of the time-mean values, the amplitude, and the phase of the fundamental harmonic of the discrete Fourier transform, the cross-correlation coefficients at zero lag, and the fraction of overall signal power at frequencies of interest. Periodic convergence is achieved when the overall fuzzy convergence level, calculated as the minimum between all the fuzzy sets, exceeds 0.95 for two consecutive cycles.

Structured grids with hexahedral cells were generated by ANSYS ICEM. The mesh independence analysis was carried out with the grid convergence index method [37]. For 2D axisymmetric simulations (one cell in the tangential direction), mesh grids comprising 11 k, 45 k, and 181 k cells were assessed. The medium mesh satisfied the independence criteria, as indicated by a grid convergence index from fine to medium mesh of 0.0014%, calculated based on the outlet Mach number. The 3D mesh was generated by revolving the 2D axisymmetric mesh of 90 deg while maintaining the same cell size of the meridional plane; the final 3D mesh is composed of 18.5 million cells.

Both ideal and non-ideal flows were simulated in the transition duct. For ideal flows, NASA polynomials were employed to consider the variation of the thermodynamic properties (specific heat, enthalpy, and entropy) with temperature [38]. Furthermore, the variation of the viscosity and thermal conductivity with temperature was modeled with the Sutherland law [39]. For non-ideal flows, thermodynamic look-up tables were built through the NIST REFPROP database [40], which offers dedicated correlations for transport properties. The accuracy of ANSYS FLUENT's flow solver in reproducing the characteristics of both supersonic and non-ideal flows is displayed by several examples in literature [24,41].

3 Method of Characteristics for Rotated Annular Asymmetric Ducts With Ideal and Non-Ideal Flows

The quasi-one-dimensional flow theory relates the Mach number and the thermodynamic quantities in the function of the local area ratio A/A^* [42]. However, this theory does not provide the optimal contour of the duct nor it considers the two-dimensionality of the flow. The method of characteristics overcomes these limitations by offering an efficient methodology to profile supersonic nozzles.

The method of characteristics (MOC) is a numerical technique for solving hyperbolic partial differential equations [43]. For steady, inviscid, two-dimensional (planar or axisymmetric), irrotational supersonic flows, which inherently exhibit hyperbolic governing equations, MOC proves to be a suitable solution method. Within the MOC framework, the governing partial differential equations are reformulated as ordinary differential equations along specific curves: these curves and the associated equations are respectively known as characteristic lines and compatibility equations. Further insights into MOC for supersonic flows can be found in the comprehensive work of Zucrow and Hoffman [43], while here only the final expressions of the characteristic lines' slope (Eq. (1)) and the compatibility equations (Eq. (2)) are reported.

$$\left(\frac{\mathrm{d}y}{\mathrm{d}x}\right)_{\pm} = \lambda_{\pm} = tan(\phi \pm \theta) \tag{1}$$

$$(V_x^2 - a^2)\,\mathrm{d}V_{x,\pm} + [2V_xV_y - (V_x^2 - a^2)\lambda_{\pm}]\,\mathrm{d}V_{y,\pm} - \frac{a^2 V_y}{y}\,\mathrm{d}x_{\pm} = 0 \tag{2}$$

Recent advancements in the implementation of the MOC have been demonstrated by Zocca et al. [44] for planar asymmetric nozzles with non-ideal flows, and by Flock and Gulhan [45] for axisymmetric nozzles featuring a constant-radius center body and with the perfect gas model. Within this work, a more general implementation of the MOC for annular asymmetric ducts rotated at an angle β with respect to the axis of symmetry and operating with flows of fluids whose properties are described by an arbitrary equation of state model is developed. The advantages of incorporating rotated channels are explained in Sec. 5; additionally, it is worth noting that implementing non-ideal flows is not mandatory for RDEs, but it is highly recommended to consider at least an ideal gas model to account for fluid property variations with temperature . Thermodynamic properties in both ideal and non-ideal flow cases are computed through the REFPROP library [40].

To initialize the solution process, three inputs are required: the flow conditions specified on an initial-value line (Sec. 3.1), the shape of the hub wall, and the shape of the shroud wall in the throat (Fig. 1). Then, the characteristic net is laid out and the correct unit process (interior point, wall point, or axis point) is applied at each intersection; the characteristic lines and the compatibility equations are solved simultaneously with the modified Euler predictor-corrector algorithm [46].

The characteristic net can be divided into three distinct regions: initial region, kernel region, and turning region. In the initial region, the characteristic lines are expanded to reach the hub wall. In the kernel region, the expansion process continues between the two walls until the desired outlet Mach number is attained on the hub. Finally, the expansion process is completed in the turning region to reach completely uniform conditions at the outlet. Furthermore, the shape of the shroud wall in the turning region is generated by the MOC by applying the continuity equation. It is worth noting that the performance of MOC-generated geometries is typically already satisfactory without the necessity of further optimizations because the profile originates directly from the governing equations.

3.1 Initial Line and Method of Characteristics Verification. The common initialization approach through Sauer's formulation [47] is not suitable since it assumes that the main flow direction is parallel to the axis of symmetry (not true for the rotated channels). Dutton and Addy [48] developed a numerically efficient and accurate method to describe the flow in the throat of rotated annular supersonic nozzles. First, the governing equations are simplified under the assumptions of a steady, inviscid, irrotational flow of a perfect gas. Then, the equations are solved with the series expansion technique, introducing transonic perturbation velocity components ($\widetilde{v_x}$ and $\widetilde{v_y}$). The resulting equations for the transonic flow in the throat are presented in Eq. (3).

$$\begin{cases} v_x = \frac{V_x}{a^*} cos(\beta) + \frac{V_y}{a^*} sin(\beta) \\ v_y = -\frac{V_x}{a^*} sin(\beta) + \frac{V_y}{a^*} cos(\beta) \\ v_x = 1 + \widetilde{v_x} = 1 + v_{x,1}\epsilon + v_{x,2}\epsilon^2 + v_{x,3}\epsilon^3 \\ v_y = \widetilde{v_y} = \left(\frac{\gamma+1}{2}\right)^{1/2} (v_{y,1}\epsilon + v_{y,2}\epsilon^2 + v_{y,3}\epsilon^3) \\ \epsilon = \frac{h''^* - g''^*}{2+\eta(h''^* - g''^*)} \end{cases} \tag{3}$$

($v_{x,1}$, $v_{y,1}$), ($v_{x,2}$, $v_{y,2}$), and ($v_{x,3}$, $v_{y,3}$) are respectively the first, second, and third-order solutions of the governing equations. Since 136 intermediate polynomial expressions are necessary for the computation of the velocity components, the complete solution is omitted here for the sake of brevity; interested readers can retrieve it in the appendix of the original report [49]. The geometrical data required for the application of this methodology are all related to the throat: the size of the throat, the inclination angle of the throat β, the first-order (h'^*, g'^*) and the second-order derivatives (h''^*, g''^*) of the hub and shroud wall in their respective throat points. In the method developed in this work, the derivatives have been calculated using a fourth-order central difference scheme.

The primary limitation of the previously described methodology lies in its assumption of a perfect gas. In an ideal gas, the isentropic coefficient γ varies with the temperature. Nevertheless, in a narrow transonic region around the throat, the variation of the isentropic coefficient is limited. Consequently, Dutton's methodology can be applied to an ideal gas by computing the isentropic coefficient at sonic conditions.

Conversely, three different isentropic exponents (γ_{pv}, γ_{Tv}, γ_{pT}) exist for non-ideal flows [10]. Wintenberger and Shepherd [3] addressed this issue by introducing the fundamental derivative of gas dynamics Γ in the derivation of Sauer's equation. However, this approach becomes impractical due to the extensive algebraic manipulations involved in Dutton's derivation. It is relevant to observe that in the derivation process, the perfect gas hypothesis is employed through the well-known closed-form isentropic flow relations. Nederstigt and Pecnik [50] demonstrated that these relations also hold for non-ideal flows with γ_{pv}, if γ_{pv} is constant. This observation holds significance as most transonic flow theories

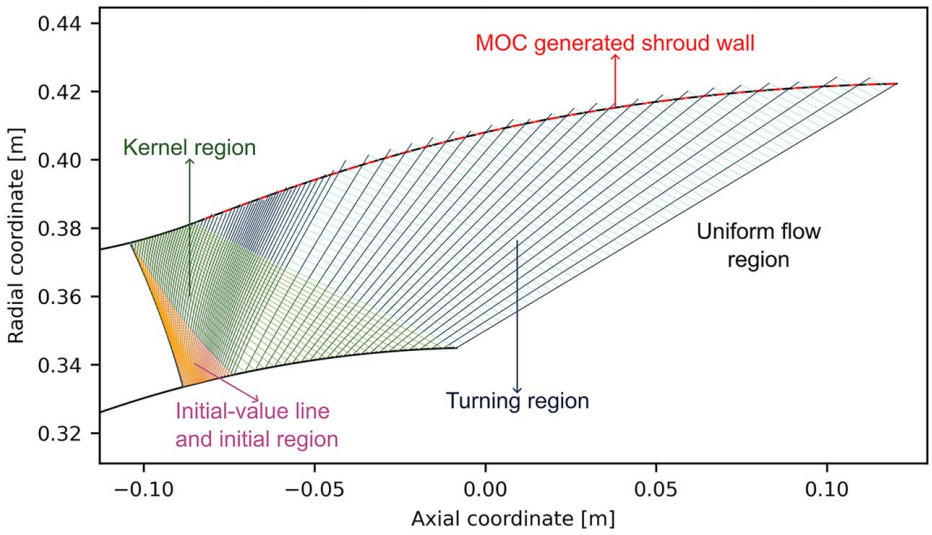

Fig. 1 Characteristic lines in a rotated annular asymmetric duct. From light to dark colors (varying grey scale in print), the characteristic lines are divided respectively into the initial region, kernel region, and turning region. The dotted line is the MOC-generated profile of the shroud wall.

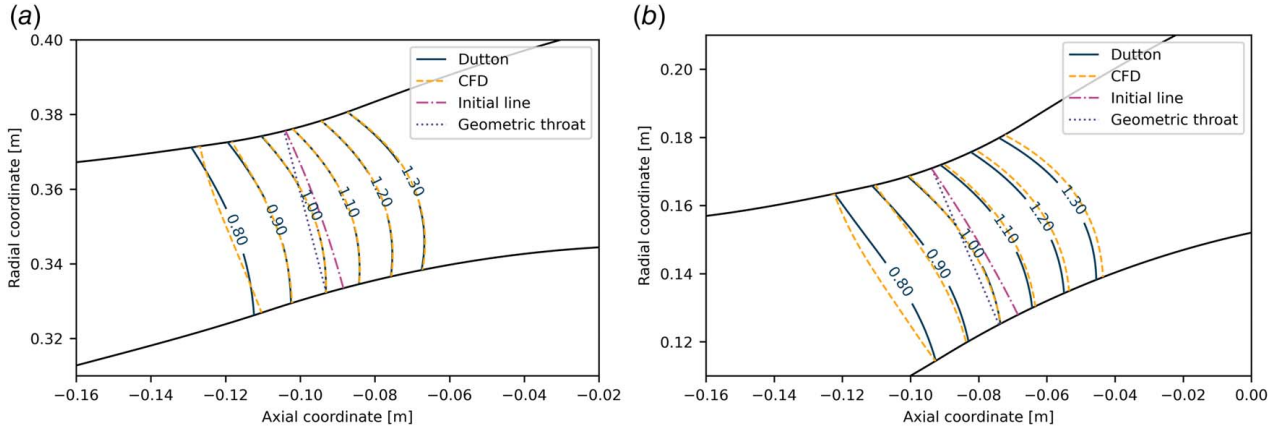

Fig. 2 Comparison between the Mach number isolines predicted with Dutton's expansion technique and the flow field obtained from inviscid 2D axisymmetric CFD simulations with (*a*) nitrogen and (*b*) siloxane MDM

are developed by employing the small perturbation technique around the throat and by assuming a perfect gas model. Hence, Dutton's and all similar methodologies can be extended to non-ideal flows by simply substituting the isentropic exponent γ with γ_{pv} (Eq. (4)).

$$\gamma_{pv} = -\frac{v}{p}\frac{c_p}{c_v}\left(\frac{\partial p}{\partial v}\right)_T \tag{4}$$

The implemented initialization method has been verified with nitrogen (ideal flow) and Siloxane MDM with a total compressibility factor Z equal to 0.65, i.e., a flow in non-ideal thermodynamic conditions. In Figs. 2(*a*) and 2(*b*), Mach number isolines predicted by the expansion technique are compared with the flow field obtained from 2D inviscid axisymmetric CFD simulations. The agreement between the analytic prediction and the CFD is excellent in both cases in the vicinity of the throat. In the ideal case, the prediction remains acceptable even up to Mach 1.3, owing to the limited variation of the isentropic coefficient. In the non-ideal case, the accuracy reduces as we move further from the throat because γ_{pv} changes significantly along the expansion process.

Once the flow in the transonic region has been generated, the initial line is built by connecting with a parabolic curve the points on the hub and shroud corresponding to the user-selected supersonic Mach numbers. It is recommended to avoid highly curved shapes for the initial line since it may lead to a characteristic line intersection upstream of the initial line itself. The maximum error between the Mach number predicted by Dutton and the one extracted from CFD along the initial lines displayed in Fig. 2 is 0.10% for nitrogen and 0.93% for MDM.

After completing the construction of the initial line, the annular rotated nozzle shape is generated with the downstream marching procedure of the MOC described in Sec. 3. The complete implementation of the method of characteristics has undergone verification for both ideal and non-ideal flows. For brevity, a single case encapsulating all MOC options within our implementation is presented here. The working fluid is Siloxane MDM, with a total pressure of 9.02 bar, a total temperature of 269 °C, and a total compressibility factor of 0.65 (reference conditions taken from Spinelli et al. [51]). The throat section has an inclination angle β of 25 deg with respect to the axis of symmetry, and the radius of the circular arc at the hub is twice the radius of the circular arc at the shroud (asymmetric duct). The outlet Mach number selected as input for the MOC is 2, and the converging section (Fig. 3) is generated with a parabolic increase of the Mach number from 0.3 at the inlet to sonic conditions). Figure 3 displays a comparison between the Mach number isolines predicted by the MOC and the results of a 2D inviscid axisymmetric CFD simulation. The excellent agreement between the two proves the correct implementation of the methodology and showcases the ability of the MOC to generate rotated asymmetric annular ducts that discharge the flow with the desired outlet Mach number.

3.2 Method of Characteristics Application for the Design of Supersonic Transition Duct for Rotating Detonation Engines. Supersonic outlet conditions were achieved experimentally by Nakata et al. [30] with a purely diverging nozzle because choking was induced by the very large heat released by the detonation combustion in a limited space. Therefore, it is not necessary to include a geometrically converging section in the design of supersonic transition ducts for RDEs. However, the method of characteristics requires accurate flow conditions on an initial line. To cope with these two requirements, a straight duct is adopted as the initial part of the transition duct (or the terminal part of the combustor). This expedient ensures that, even though the precise location of the thermal choking is unknown, sonic conditions are guaranteed at the inlet of the diverging section.

The combustion products are computed using the NASA-CEA software in detonation mode [52] and they are treated as an ideal gas. A total pressure of 15 bar, a total temperature of 2340 K, and a mass flowrate of 100 kg/s are selected considering typical quantities for RDEs and high-pressure turbines [5,8,15,26,28,31]. In the baseline geometry, the inclination angle β of the throat is set to 0 deg, and a constant radius of 0.345 m is assigned to the hub. The shroud radius is determined through mass flowrate conservation, while the shroud profile at the throat is a circle with a radius identical to that of the hub (Fig. 4). The Mach number selected as the outlet condition of the transition duct is 2 (this choice will be justified in Sec. 5).

Dutton's methodology, akin to other similar techniques, is based on the underlying assumption that the flow is continuously accelerating from the converging section to the diverging one.

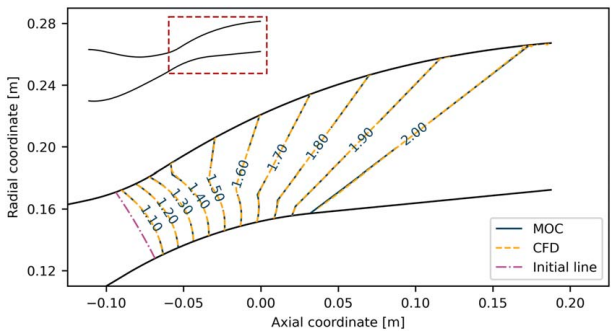

Fig. 3 Comparison between the Mach number isolines predicted by the method of characteristics and the flow field obtained from an inviscid 2D axisymmetric CFD simulation with Siloxane MDM.

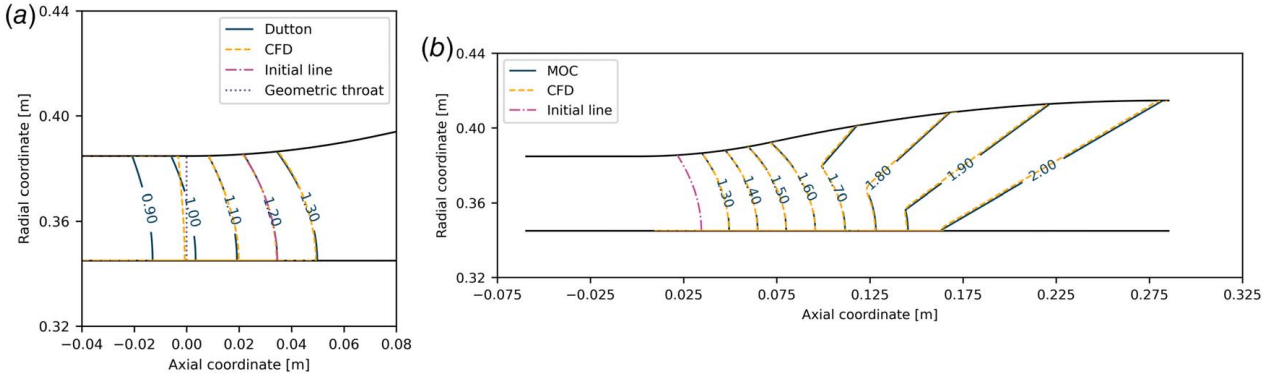

Fig. 4 Comparison between the Mach number isolines predicted by the analytic methods ((*a*) Dutton's expansion technique and (*b*) method of characteristics) and the flow field obtained from the 2D inviscid axisymmetric CFD simulation of the supersonic transition duct.

However, in the straight region of the duct, the sonic Mach number remains constant after thermally choking. In addition, the throat is not geometrically well-defined, as all the sections in the straight duct can be considered a throat in an inviscid case. These factors have an impact on the accuracy of Dutton's methodology, especially in the section that separates the straight region from the diverging one. As observed in Sec. 3.1, for an ideal gas, the flow field predicted by Dutton's expansion technique maintains acceptable accuracy up to Mach 1.3. Hence, the Mach number selected for the initial line is 1.2 to move away from the critical section. Furthermore, the derivatives at the throat hub and shroud points are calculated with a third-order right-sided difference scheme to avoid considering the straight portion of the duct. With these adjustments, the maximum error between the Mach number predicted by Dutton and the 2D inviscid axisymmetric simulation along the initial line is reduced to 0.16%. Finally, Figs. 4(*a*) and 4(*b*) provide a comparison between the Mach number isolines predicted by the analytic methods and the flow field extracted from the CFD simulation.

4 Viscous Effects in Supersonic Transition Ducts

The profile of the supersonic transition duct was generated with the inviscid MOC, and the flow evolution within the channel was verified with inviscid CFD simulations (Sec. 3). To consider the influence of boundary layers, a viscous 2D axisymmetric simulation has been performed on the same geometry (Fig. 6). The Mach number isolines exhibit downstream shifting because of the boundary layer growth; however, the overall impact of boundary layers on the flow field is relatively modest.

In a design-oriented approach, it is valuable to provide an accurate estimate of the losses. The main source of loss generation in the transition duct arises from viscous dissipation within the hub and shroud boundary layers. An additional source of entropy production is the mixing of the highly non-uniform flow introduced by the combustor. In this work, the entropy produced by the mixing of the non-uniformities generated by the combustor is not attributed to the transition duct, following the mixed-out flow approach [53]. On the other hand, the supersonic channel is responsible for amplifying the non-uniformities at the inlet or for generating new ones. However, this contribution is deemed negligible compared to the viscous dissipation resulting from extremely high velocities.

The entropy production is calculated with Eq. (5), proposed by Denton [54] and specifically derived for axisymmetric geometries. ρ_{fs}, V_{fs}, T_{fs} are the freestream quantities obtained from the MOC results, while C_d stands for the entropy dissipation coefficient.

$$\Delta s = \frac{2\pi}{\dot{m}} \int_{x_{inlet}}^{x_{outlet}} C_d(x)\rho_{fs}(x)\frac{V_{fs}^3(x)}{T_{fs}(x)} y(x)\sqrt{y'^2(x)+1}\,\mathrm{d}x \tag{5}$$

Typically, the dissipation coefficient is determined using Eq. (6) developed by Moore and Moore [55], after calculating the momentum thickness with the correlations presented by Stratford and Beavers for compressible turbulent boundary layers [56]. The total entropy production predicted through Eqs. (5) and (6) is 18.82 J/(kg K), which is 31.2% higher than the entropy rise extracted from the CFD simulation (14.34 J/(kg K)). This difference can be explained by the observation that correlations for the dissipation coefficient tend to overpredict the losses when applied to accelerating flows [54].

$$C_d = 0.0056\mathrm{Re}_\theta^{-1/6} \tag{6}$$

To overcome the limit of applicability of traditional correlations, the boundary layer quantities are determined by coupling the in-house boundary-layer code BLnI with the MOC. The algebraic zero-equation eddy viscosity model by Cebeci and Smith [57] is employed for turbulence closure, and the thermo-physical fluid properties are computed through the REFPROP library [40]. Since the boundary layer code has been developed in previous works, a comprehensive description is omitted here, but the reader can find a detailed presentation in Ref. [58].

As displayed in Fig. 5, the dissipation coefficient computed by the boundary layer code is notably smaller than the value obtained with Truckenbodt's correlations. The entropy production estimated with the updated value of C_d is 14.81 J/(kg K), which is 3.2% higher than CFD. This variation can be partially explained by the different turbulent models employed in CFD and BLnI.

Since the pressure gain is one of the main advantages of rotating detonation combustors, it is relevant to also quantify the percentage of pressure gain lost within the supersonic transition duct. Total pressure losses are evaluated with Eq. (7), which is a standard definition applied for ducts [59]. The outlet total pressure is determined

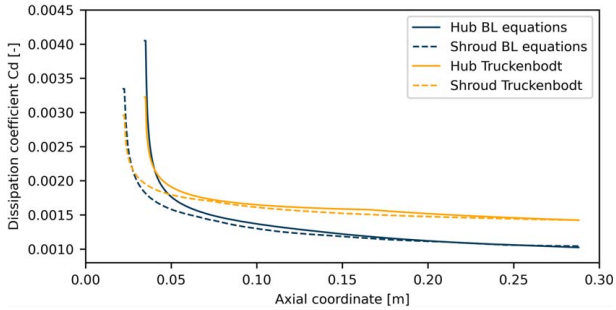

Fig. 5 Comparison between the dissipation coefficient C_d estimated with Truckenbodt's correlations and the values computed by the boundary layer code.

by characterizing a mixed-out thermodynamic state, assuming total enthalpy conservation (adiabatic walls) and the entropy increase predicted with the boundary layer code. The total pressure loss ξ calculated with the boundary layer code is 4.20%, which is slightly higher than the 3.73% value obtained from the viscous steady-state CFD simulation.

$$\xi = \frac{p_{t,in} - p_{t,out}}{p_{t,in}} \tag{7}$$

Among other relevant quantities, the boundary layer code provides also the values of the boundary layer thickness, that can be used to correct the transition duct profile generated with the inviscid MOC. Typically, the displacement thickness is selected for correcting the profile of a converging–diverging nozzle; the reason behind this choice is to maintain the desired mass flowrate by compensating the boundary layer growth. However, in a transition duct for RDEs, the mass flowrate does not vary if the effective area is increased in the diverging portion of the channel because of thermal choking. Consequently, the hub and shroud profile are displaced by the momentum thickness to obtain the desired Mach number at the outlet section. Figure 6 illustrates how the agreement between the Mach number isolines of the viscous CFD simulations and the MOC is notably improved for the corrected geometry compared to the baseline.

In conclusion, the coupling of the method of characteristics with a boundary layer code has proven to be effective for accurately estimating losses and refining the profile without the need for CFD simulations. These tools are particularly valuable during the preliminary design phase when multiple designs are under consideration.

5 Unsteady Effects in Supersonic Transition Ducts

The flow delivered by the rotating detonation combustor is characterized by significant fluctuations across all thermodynamic quantities. Mushtaq et al. [19] observed that the Mach number and inlet flow angle fluctuations have a large impact on the performance of a supersonic inlet turbine; supersonic blade entropy production increases by 60% for a 0.5 Mach number rise over the design value, and by 40% for 10 deg of incidence angle. Therefore, it is necessary to implement methodologies capable of predicting the maximum incidence and the unsteadiness in the Mach number at the turbine inlet. Furthermore, these methodologies, systematically applied, are the basis for the development of design guidelines for transition ducts capable of attenuating these adverse flow effects.

The maximum incidence angle at the inlet of the turbine is predicted with a reduced order model (ROM) proposed by Agromayor et al. [60], based on the assumptions of a one-dimensional steady-state axisymmetric flow in the meridional direction. The evolution of the flow angle α, defined with respect to the meridional direction, is predicted by solving mass, momentum, and energy equations (Eq. (8)). The input data required to solve the ordinary differential equations are the geometry of the duct and the boundary conditions at the inlet section.

$$\begin{cases} V_m \frac{\mathrm{d}\rho}{\mathrm{d}m} + \rho \frac{\mathrm{d}V_m}{\mathrm{d}m} = \frac{\rho V_m}{yb} \frac{\mathrm{d}(by)}{\mathrm{d}m} \\ \rho V_m \frac{\mathrm{d}V_m}{\mathrm{d}m} + \frac{\mathrm{d}p}{\mathrm{d}m} = \frac{\rho V_z^2}{y} sin(\phi) - \frac{1}{2}\rho V^2 \left(\frac{C_{f,h} y_h + C_{f,sh} y_{sh}}{y} \right) \frac{cos(\alpha)}{b} \\ \rho V_m \frac{\mathrm{d}V_z}{\mathrm{d}m} = -\frac{\rho V_z V_m}{y} sin(\phi) - \frac{1}{2}\rho V^2 \left(\frac{C_{f,h} y_h + C_{f,sh} y_{sh}}{y} \right) \frac{sin(\alpha)}{b} \\ \rho V_m \frac{\mathrm{d}p}{\mathrm{d}m} - \rho V_m a^2 \frac{\mathrm{d}\rho}{\mathrm{d}m} = \frac{\frac{1}{2}\rho V^2 (C_{f,h} y_h + C_{f,sh} y_{sh}) V}{b \left(\frac{\partial e}{\partial p} \right)_\rho} \end{cases} \tag{8}$$

The ROM has been applied to both subsonic and supersonic channels. For the supersonic cases, the duct is generated with the MOC and the skin friction coefficient C_f is computed by the boundary layer code. For the subsonic cases, a conical annular diffuser with a 5 deg divergence semi-angle is produced, and the skin friction coefficient is 0.005 [61]. At the inlet, an axial Mach number of 1.01 and 0.99 is assigned for supersonic and subsonic cases, respectively (the system of equations is not invertible for a sonic axial Mach number [60]). Braun et al. [28] and Nassini et al. [10] reported fluctuations for the inlet flow angle α on the order of $\pm$25 deg. Since the ROM assumes stationary flow, a conservative approach is adopted by selecting a steady value of the inlet flow angle equal to 25 deg for both subsonic and supersonic cases; hence, the flow angle computed by the ROM at the outlet is representative of the maximum flow angle as seen by the turbine.

The relation between the maximum outlet flow angle α and the outlet Mach number is illustrated in Fig. 7. Starting from the baseline case with no throat inclination angle β, the stream tubes are axially stretched or compacted due to flow acceleration or deceleration in the duct. Since the variation of the tangential component of the velocity is limited to viscous dissipation (the mean radius is constant for $\beta = 0$ deg), the increase of the axial velocity in the supersonic duct allows a relevant reduction in the maximum outlet flow angle, thus improving turbine inlet conditions. Conversely, flow deceleration in the subsonic channel leads to a significant increase in the flow angle; these results suggest the importance of robust optimization of subsonic turbines in RDEs.

The effect of the throat inclination angle β is clarified in Fig. 8, where two MOC-generated supersonic ducts, each with an outlet

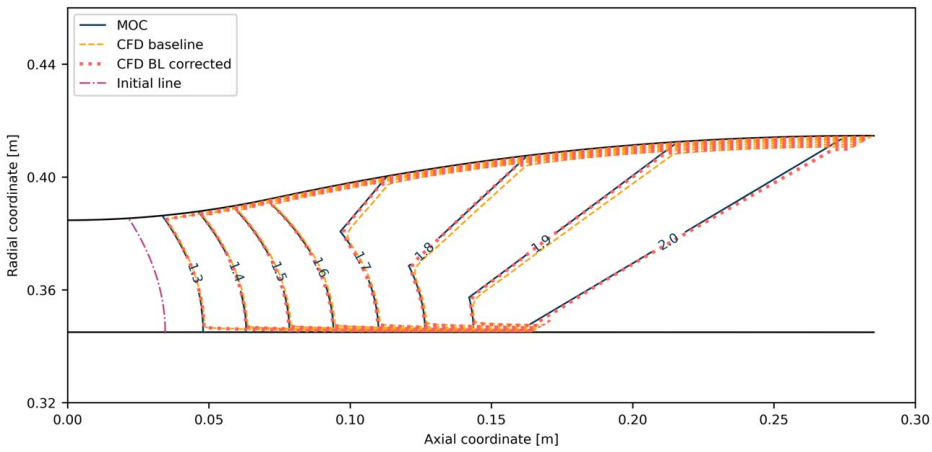

Fig. 6 The Mach fields obtained from the 2D viscous axisymmetric CFD simulations of the baseline transition duct geometry and the one corrected for the momentum thickness are compared to the Mach number isolines of the MOC.

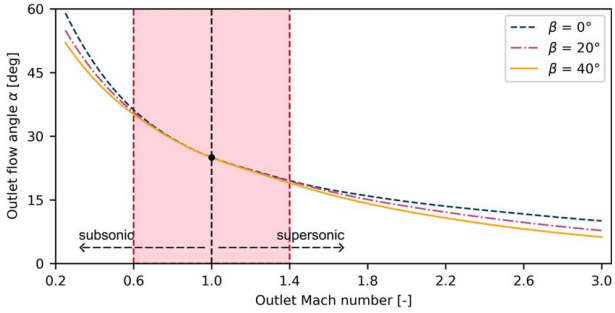

Fig. 7 The trend of the maximum flow angle α with respect to the outlet Mach number. The curves are parameterized in function of the inclination angle β.

Mach number of 2 but constructed with different inclination angles, are compared. According to radial equilibrium, in the rotated channel the increase in the mean radius lowers the tangential component of the velocity, which in turn reduces the maximum outlet flow angle. Specifically, for an outlet Mach number of 2 and an inclination angle of 30 deg, the maximum outlet flow angle is diminished by 25% compared to the non-rotated geometry. However, the effect of β on α is non-linear: relevant reductions compared to the $\beta = 0$ deg case are observed only for Mach numbers lower than 0.6 or higher than 1.4 (Fig. 7), which aligns with the range of interest for turbines in RDEs (Sec. 1).

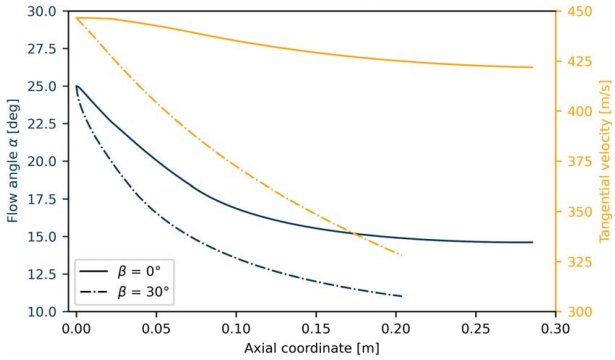

Fig. 8 Comparison in terms of flow angle α and tangential velocity component between a non-rotated and a rotated supersonic MOC-generated transition duct with an outlet Mach number of 2.

Furthermore, rotated channels provide additional flexibility for the engine architecture, by reducing the axial size of the machine at the expense of the radial one (Fig. 8) and by increasing the peripheral velocity of the turbine. These benefits justify the importance of appropriate design methodologies based on MOC for rotated supersonic annular ducts.

Two-dimensional axisymmetric inviscid unsteady simulations have been performed to study and estimate the damping of the fluctuations in the supersonic duct when subjected to time-varying inlet conditions. The reference geometry has been described in Sec. 3 and corrected for the boundary layer thickness. Inviscid simulations are considered adequate since Braun et al. [27] observed that Euler simulations overpredicted the damping in the fluctuations by only 3% compared to URANS.

The inlet Mach number was varied in time with a sinusoidal function (Eq. (9)). The average Mach number $\bar{M}$ was set to 1.35, the amplitude of the fluctuations A was 0.15 (unsteadiness level reported by Nassini et al. [10]), and several frequencies f were tested. The static pressure and static temperature were maintained constant, while the total quantities changed according to the Mach number.

$$M(t) = \bar{M} + A\sin(2\pi ft) \tag{9}$$

The Mach number increase and decrease produce compression and rarefaction waves, propagating as left $(V_x - a)$ and right running $(V_x + a)$ characteristics (note that these characteristics refer to the unsteady one-dimensional solution of the governing equations). The response of the supersonic duct to unsteady inlet conditions is influenced by two physical effects: the strength of the pressure waves and their interaction between consecutive periods. It is well known that rarefaction waves progressively broaden whereas compression waves progressively coalesce and tend to form a compression shock [62]. The coalescence of pressure waves is more pronounced for the high-frequency cases because smaller periods lead to larger spatial gradients and ultimately stronger pressure waves (Fig. 9).

The intensity of Mach number fluctuations along the channel was quantified by computing the standard deviation σ_M in time on vertical monitor lines evenly spaced from inlet to outlet. The motion and the interaction of the strong pressure waves generated in the high-frequency cases are responsible for the complex trends of σ_M displayed in Fig. 9(*a*). It is interesting to observe that the damping of the sinusoidal inlet conditions shows a non-monotonic relationship with both frequency and axial position. The results can be summarized based on the definition of the reduced frequency $\bar{f}$

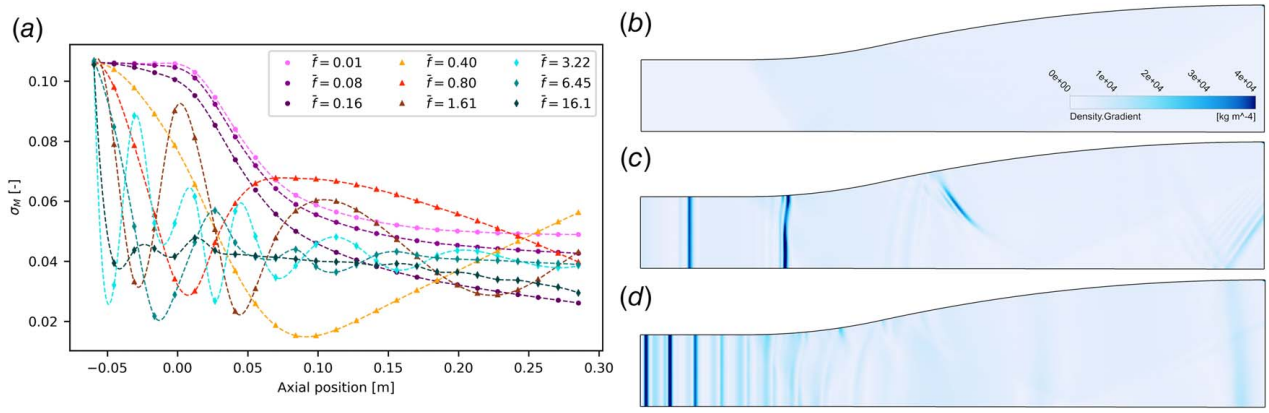

Fig. 9 (*a*) Trend of the standard deviation of the Mach number σ_M in time along the channel with a sinusoidal fluctuation of the inlet Mach number. The cases are classified in three categories: dots for $\bar{f} << 1$, triangles for $\bar{f} \sim 1$, and diamonds for $\bar{f} >> 1$. (*b*)–(*d*) display the spatial density gradient contours for three cases, each of them representative of a category. The motion and the interaction of the strong pressure waves generated in the high-frequency cases are responsible for the complex trends of σ_M.

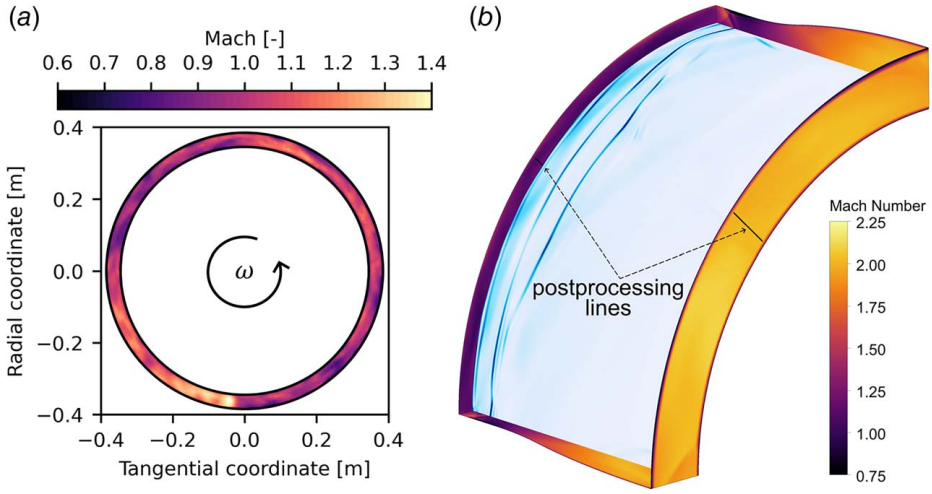

Fig. 10 (*a*) Mach field assigned at the inlet of the transition duct in the 3D viscous simulation, (*b*) Mach field at the inlet, outlet, and periodic boundaries, along with the density gradient contours on the mean radius surface.

(Eq. (10)).

$$\bar{f} = \frac{f}{\frac{V_{x-in}}{L_x}} \tag{10}$$

For $\bar{f} << 1$ (Fig. 9(*b*)), a quasi-steady behavior is observed within the channel: the pressure waves are weak, and the intensity of the Mach number fluctuations monotonically decrease from inlet to outlet. For $\bar{f} \sim 1$ (Fig. 9(*c*)), stronger pressure waves form compression shocks. The interaction between consecutive periods is limited since they are sufficiently far apart. For $\bar{f} >> 1$ (Fig. 9(*d*)), the fluctuations associated to consecutive periods are considerably closer in space. This proximity allows the interaction between the strong rarefaction and compression waves generated in different temporal periods, mitigating the level of unsteadiness of the Mach number at the outlet of the domain.

If the reduced frequency is significantly lower than 1 or higher than 1, the damping of the Mach number fluctuations can be conservatively approximated to the quasi-steady value, easily calculated through two steady-state simulations (Eq. (11)). On the contrary, if $\bar{f} \sim 1$, an unsteady simulation is necessary due to the potential amplification of fluctuations resulting from the interaction between pressure waves. Ultimately, the development of a reduced-order model capable of estimating the damping factor given the frequency of the inlet fluctuation would eliminate the necessity of performing simulations, even for reduced frequencies closer to the unitary value.

$$\mu = \frac{\Delta M_{outlet}}{\Delta M_{inlet}} = 0.46 \tag{11}$$

Furthermore, these simulations provide valuable information on the losses generated due to the mixing of the unsteady inlet conditions, while excluding the viscous contribution at the walls. Higher frequencies generally result in an increased entropy production, but the most significant finding is that the mixing losses are nearly two orders of magnitude smaller than viscous losses at the walls. This justifies the choice of considering only viscous dissipation on the walls in calculating duct losses during the preliminary design phase. It should be noted that two contributions are not addressed by these simulations: mixing associated with spatially non-uniform inlet conditions and the impact of turbulent mixing. However, as discussed in Sec. 4, the first contribution should be attributed to the combustor rather than the downstream components.

Finally, an unsteady 3D viscous simulation was carried out to verify the accuracy of the proposed reduced-order models. RDC-representative inlet conditions were extracted from the large eddy simulation (LES) carried out by Nassini et al. [10] on the

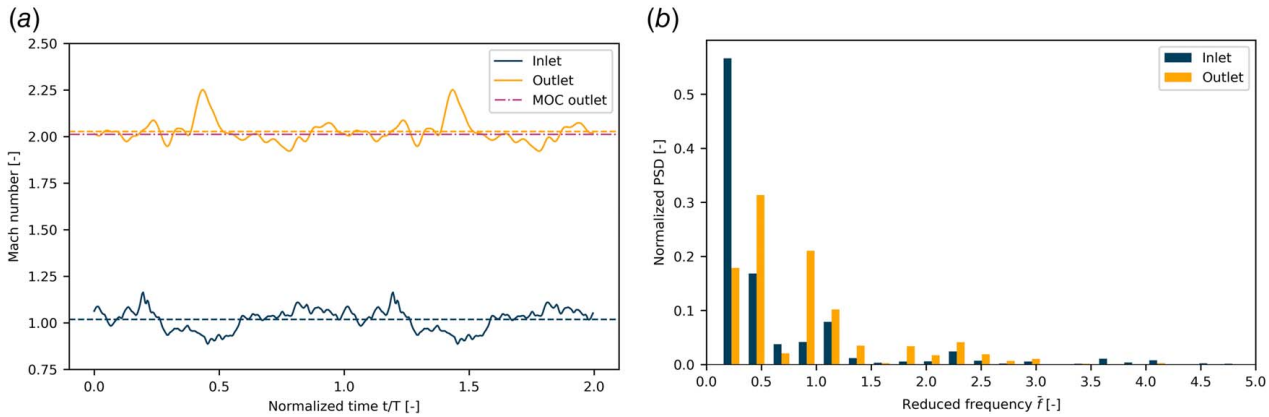

Fig. 11 (*a*) Line-averaged inlet and outlet Mach numbers along a reference line oriented at a 45 deg angle with respect to the periodic boundary conditions. The dashed line represents the temporal average, and (*b*) normalized power spectral density of the inlet and outlet Mach numbers.

combustor installed at TU Berlin. From the LES simulation, the same Mach field (Fig. 10(*a*)) and the same flow angles have been prescribed, while the non-uniformities in pressure and temperature have been mapped onto our mean values. Then, the inlet conditions were placed on a rotating frame of reference with a rotational speed equal to the detonation wave speed measured by Nassini (1942 m/s).

Despite the coalescence of compression waves in the initial part of the channel due to the high-frequency content in the inlet conditions, the contour of the Mach number displays that the flow field appears almost uniform at the outlet section (Fig. 10(*b*)). For the characterization of turbine inlet conditions and evaluation of ROM accuracy, the trend of the Mach number and the flow angles are extracted along two lines (for the inlet and the outlet) placed at 45 deg with respect to the periodic boundary conditions. Figure 11(*a*) shows that the transonic flow at the inlet is accelerated and exits the duct at an average outlet Mach number of 2.03. This demonstrates the ability of MOC-generated ducts to obtain the desired outlet Mach number even under non-uniform inlet conditions in time and space. Furthermore, the power spectral density has been calculated for both inlet and outlet Mach numbers (Fig. 11(*b*)). The results confirm the findings from inviscid axisymmetric simulations: low and high reduced frequencies are damped, while the damping or amplification of the reduced frequencies close to the unitary value depends on how pressure waves interact. The flow angles α reduce from inlet to outlet due to flow acceleration; the difference between the maximum and minimum outlet flow angle predicted by the 1D model, determined by assigning as input the maximum and minimum inlet flow angle, and the corresponding values obtained from the CFD simulation is 1.6 deg and 0.14 deg (Fig. 12).

Finally, the total pressure reduction ξ in the channel is 4.49%, including the losses associated with the mixing of the non-uniform inlet conditions. The agreement with the reduced-order model prediction is satisfactory with a deviation of only 0.29%. This loss value provides a quantification of the share of pressure gain dissipated within the transition duct. Such information is of utmost importance for assessing the feasibility of gas turbine architectures integrating rotating detonation combustors and supersonic turbines.

In summary, careful consideration should be given to the choice of the transition duct outlet Mach number to prevent the occurrence of incidence angles that may compromise turbine performance. While the frequency content of the RDC outlet flow conditions depends strongly on the number of detonation waves in the combustor, the reduced frequencies can be effectively modified by increasing or decreasing the length of the channel exploiting the degrees-of-freedom in the method of characteristics.

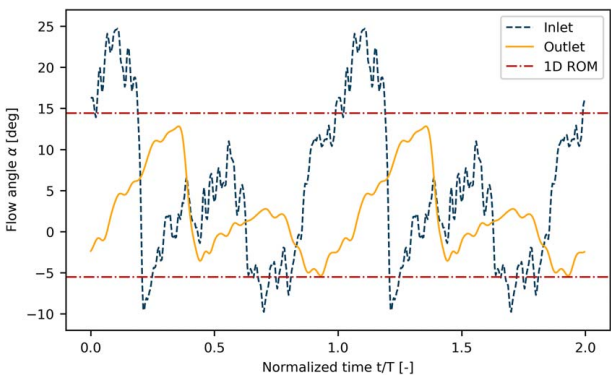

Fig. 12 Line-averaged inlet and outlet flow angles α along a reference line oriented at a 45 deg angle with respect to the periodic boundary conditions. The dashed-dotted line represents the maximum and minimum outlet flow angle predicted by the 1D ROM model.

6 Conclusions

The supersonic transition duct is a critical component of a rotating detonation engine featuring a supersonic inlet turbine. While prior investigations on the topic have considered only simplified designs of the supersonic nozzle of the turbine, this paper presents an efficient methodology for the design of the supersonic transition duct, embedding a reduced-order model for loss quantification. A simplified method for predicting and mitigating the unsteadiness in the flow delivered to the turbine is also documented.

The method of characteristics for planar nozzles has been extended for generating the profile of a rotated annular asymmetric duct accommodating fluids with properties defined by an arbitrary equation of state model. The initialization method, based on Dutton's expansion technique, has been extended to non-ideal flows through the isentropic exponent γ_{pv}. The agreement between the Mach number isolines predicted by the MOC and the results of 2D inviscid axisymmetric CFD simulations is satisfactory. Since conventional correlations for the dissipation coefficient are inadequate for accelerating flows, an accurate estimate of the viscous entropy production is obtained by coupling a boundary layer solver with the method of characteristics.

The transition duct outlet flow angle is predicted with a one-dimensional reduced-order model. Flow angle fluctuations are considerably amplified in decelerating channels, reaching values up to 60 deg when 25 deg is assigned at the inlet; on the contrary, supersonic channels reduce the flow angles, thus improving turbine inlet conditions. The propagation of the inlet fluctuations along the duct is studied through 2D axisymmetric unsteady CFD simulations. The response of the supersonic transition duct to unsteady inlet conditions can be summarized as follows: if the reduced frequency is significantly lower than 1 or higher than 1, the damping of the Mach number fluctuations can be conservatively approximated to the quasi-steady value. Inlet fluctuations with a reduced frequency near unity are subject to amplification or damping based on the interaction among the different pressure waves traveling in the channel. The accuracy of the reduced-order models is verified through an unsteady 3D viscous simulation of the flow within the transition duct under RDC-representative inlet conditions.

In summary, the work demonstrated that supersonic transition ducts whose profile is designed through a generalized MOC supplemented by a physics-based reduced-order model for the estimation of the losses provide nearly uniform flow at the inlet of supersonic turbines in RDEs. It is therefore envisaged that the developed design methodology can be used in system-level analyses and optimization studies integrating models of the RDC and the supersonic inlet turbine.

Acknowledgment

The authors express their gratitude to Professor Andreini and Dr. Nassini for generously providing the data necessary to evaluate the accuracy of the reduced-order model under RDC-representative inlet conditions.

Conflict of Interest

There are no conflicts of interest.

Data Availability Statement

The datasets generated and supporting the findings of this article are obtainable from the corresponding author upon reasonable request.

Nomenclature

a = speed of sound (m/s)
e = specific energy (J/kg)

g = shroud wall contour (m)
h = hub wall contour (m)
p = pressure (Pa)
s = specific entropy (J/(kg K))
v = dimensionless velocity or volume (m^3)
A = amplitude of the fluctuation or area (m^2)
M = Mach number
T = temperature (K)
V = velocity (m/s)
$\dot{m}$ = mass flowrate (kg/s)
C_d = entropy dissipation coefficient
C_f = skin friction coefficient
f, $\bar{f}$ = frequency and reduced frequency (Hz and –)
C_p, C_v = specific heat at constant pressure and volume (J/(kg K))
x, y, z = axial, radial, and tangential coordinates (m)
α = angle between velocity and meridional velocity (deg)
β = throat inclination angle (deg)
γ = isentropic coefficient
ϵ = expansion parameter
η = parameter in expansion variable
θ = Mach angle or momentum thickness (deg or m)
λ = characteristic line slope
μ = static damping ratio
ξ = total pressure reduction
ρ = density (kg/m^3)
ϕ = angle between axial and meridional velocity (deg)
$()_{fs}$ = freestream conditions
$()_m$ = meridional component
$()^*$ = sonic throat conditions
CFD = computational fluid dynamics
MOC = method of characteristics
RDC = rotating detonation combustor
RDE = rotating detonation engine
ROM = reduced order model

References

[1] Wolański, P., 2013, "Detonative Propulsion," Proc. Combust. Inst., **34**(1), pp. 125–158.
[2] Jones, S. M., and Paxson, D. E., 2013, "Potential Benefits to Commercial Propulsion Systems From Pressure Gain Combustion," 49th AIAA/ASME/SAE/ASEE Joint Propulsion Conference, San Jose, CA, July 14–17.
[3] Wintenberger, E., and Shepherd, J. E., 2006, "Thermodynamic Cycle Analysis for Propagating Detonations," J. Propul. Power, **22**(3), pp. 694–698.
[4] Frolov, S. M., Dubrovskii, A. V., and Ivanov, V. S., 2013, "Three-Dimensional Numerical Simulation of Operation Process in Rotating Detonation Engine," Progr. Propul. Phys., **4**, pp. 467–488.
[5] Sousa, J., Paniagua, G., and Collado Morata, E., 2017, "Thermodynamic Analysis of a Gas Turbine Engine With a Rotating Detonation Combustor," Appl. Energy, **195**, pp. 247–256.
[6] Anand, V., and Gutmark, E., 2019, "Rotating Detonation Combustors and Their Similarities to Rocket Instabilities," Prog. Energy Combust. Sci., **73**, pp. 182–234.
[7] Sarraf, D. K., and Spencer, D., 2023, "BP Energy Outlook 2023". Technical Report, Bretish Petroleum.
[8] Ma, J. Z., Luan, M. -Y., Xia, Z. -J., Wang, J. -P., Zhang, S.-j., Yao, S.-b., and Wang, B., 2020, "Recent Progress, Development Trends, and Consideration of Continuous Detonation Engines," AIAA J., **58**(12), pp. 4976–5035.
[9] Raman, V., Prakash, S., and Gamba, M., 2023, "Nonidealities in Rotating Detonation Engines," Annu. Rev. Fluid Mech., **55**(1), pp. 639–674.
[10] Nassini, P. C., Andreini, A., and Bohon, M. D., 2023, "Characterization of Refill Region and Mixing State Immediately Ahead of a Hydrogen-Air Rotating Detonation Using LES," Combust. Flame, **258**, p. 113050.
[11] Liu, Z., Braun, J., and Paniagua, G., 2020, "Integration of a Transonic High-Pressure Turbine With a Rotating Detonation Combustor and a Diffuser," Int. J. Turbo Jet-Engines, **40**(1), pp. 1–10.
[12] Kantrowitz, A., and Donaldson, C., 1945, "Preliminary Investigation of Supersonic Diffusers". NACA Wartime Reports.
[13] Mushtaq, N., and Gaetani, P., 2023, "Understanding and Modeling Unstarting Phenomena in a Supersonic Inlet Cascade," Phys. Fluids, **35**, p. 106101.
[14] Starken, H., Yongxing, Z., and Schreiber, H.-A., 1984, "Mass Flow Limitation of Supersonic Blade Rows Due to Leading Edge Blockage".
[15] Paniagua, G., Iorio, M. C., Vinha, N., and Sousa, J., 2014, "Design and Analysis of Pioneering High Supersonic Axial Turbines," Int. J. Mech. Sci., **89**, pp. 65–77.
[16] Mushtaq, N., Colella, G., and Gaetani, P., 2022, "Design and Parametric Analysis of a Supersonic Turbine for Rotating Detonation Engine Applications," Int. J. Turbomach., Propul. Power, **7**(1), p. 1.
[17] Inhestern, L. B., Braun, J., Paniagua, G., and Serrano Cruz, J. R., 2020, "Design, Optimization, and Analysis of Supersonic Radial Turbines," ASME J. Eng. Gas Turbines Power, **142**(3), p. 031023.
[18] Sousa, J., and Paniagua, G., 2015, "Entropy Minimization Design Approach of Supersonic Internal Passages," Entropy, **17**(8), pp. 5593–5610.
[19] Mushtaq, N., Persico, G., and Gaetani, P., 2023, "The Role of Endwall Shape Optimization in the Design of Supersonic Turbines for Rotating Detonation Engines," ASME J. Turbomach., **145**(8), p. 081015.
[20] Sousa, J., Paniagua, G., and Saavedra, J., 2017, "Aerodynamic Response of Internal Passages to Pulsating Inlet Supersonic Conditions," Comput. Fluids, **149**, pp. 31–40.
[21] Mushtaq, N., and Gaetani, P., 2024, "The Effect of Upstream Unsteadiness on the Unstarting of a Supersonic Inlet Turbine," ASME J. Turbomach., **146**(4), p. 041005.
[22] Braun, J., Liu, Z., Cuadrado, D., Andreoli, V., Paniagua, G., Saavedra, J., Athmanathan, V., and Meyer, T. R., 2019, "Characterization of an Integrated Nozzle and Supersonic Axial Turbine With a Rotating Detonation Combustor," AIAA Propulsion and Energy 2019 Forum, Indianapolis, IN, Aug. 19–22, pp. 1–11.
[23] Shen, D., Cheng, M., Wu, K., Sheng, Z., and Wang, J., 2022, "Effects of Supersonic Nozzle Guide Vanes on the Performance and Flow Structures of a Rotating Detonation Combustor," Acta Astronaut., **193**, pp. 90–99.
[24] Su, L., Wen, F., Wan, C., Han, J., Wang, Y., and Wang, S., 2023, "Coupling Study of Supersonic Turbine Stage and Two-Dimensional Hydrogen/Air Rotating Detonation Combustor," Phys. Fluids., **35**(6), p. 66125.
[25] Bach, E., Paschereit, C. O., Stathopoulos, P., and Bohon, M. D., 2021, "Rotating Detonation Wave Direction and the Influence of Nozzle Guide Vane Inclination," AIAA J., **59**(12), pp. 5276–5287.
[26] Braun, J., Saracoglu, B. H., and Paniagua, G., 2017, "Unsteady Performance of Rotating Detonation Engines With Different Exhaust Nozzles," J. Propul. Power, **33**(1), pp. 121–130.
[27] Braun, J., Saavedra, J., and Paniagua, G., 2017, "Evaluation of the Unsteadiness Across Nozzles Downstream of Rotating Detonation Combustors," 55th AIAA Aerospace Sciences Meeting, Grapevine, TX, Jan. 9–13, pp. 1–12.
[28] Braun, J., Paniagua, G., and Ferguson, D., 2021, "Aero-Thermal Characterization of Accelerating and Diffusing Passages Downstream of Rotating Detonation Combustors," ASME Turbo Expo 2021, p. GT2021–59111.
[29] Nakata, K., Ota, K., Ito, S., Ishihara, K., Goto, K., Itouyama, N., Watanabe, H., Kawasaki, A., Matsuoka, K., Kasahara, J., and Matsuo, A., 2022, "Supersonic Exhaust From a Rotating Detonation Engine With Throatless Diverging Channel," AIAA J., **60**(7), pp. 4015–4023.
[30] Nakata, K., Ishihara, K., Goto, K., Itouyama, N., Watanabe, H., Kawasaki, A., Matsuoka, K., et al., 2023, "Experimental Investigation of Inner Flow of a Throatless Diverging Rotating Detonation Engine," Proc. Combust. Inst., **39**(3), pp. 3073–3082.
[31] Sun, C., Zheng, H., Zhao, N., Li, Z., and Zhu, W., 2021, "Performance Evaluation and Outlet Load Improvement of a Rotating Detonation Combustor With Different Outlet Nozzles," Int. J. Hydrogen Energy, **46**(35), pp. 18644–18660.
[32] Ansys, 2020. "ANSYS Fluent Theory Guide".
[33] Leonard, B., and Mokhtari, S., 1990, "ULTRA-SHARP Nonoscillatory Convection Schemes for High-Speed Steady Multidimensional Flow". Technical Report, NASA.
[34] Menter, F. R., 1994, "Two-Equation Eddy-Viscosity Turbulence Models for Engineering Applications," AIAA J., **32**(8), pp. 1598–1605.
[35] Shannon, C. E., 1948, "A Mathematical Theory of Communication," Bell Syst. Technol. J., **27**(3), pp. 379–423.
[36] Clark, J. P., and Grover, E. A., 2006, "Assessing Convergence in Predictions of Periodic-Unsteady Flowfields," ASME J. Turbomach., **129**(4), pp. 740–749.
[37] Celik, I. B., Ghia, U., Roache, P. J., Freitas, C. J., Coleman, H., and Raad, P. E., 2008, "Procedure for Estimation and Reporting of Uncertainty Due to Discretization in CFD Applications," ASME J. Fluids Eng., **130**(7), p. 078001.
[38] McBride, B. J., 2002, 'NASA Glenn Coefficients for Calculating Thermodynamic Properties of Individual Species. National Aeronautics and Space Administration, John H. Glenn Research Center.
[39] Sutherland, W., 1893, "LII. The Viscosity of Gases and Molecular Force," Lond. Edinb. Dublin Phil. Mag. J. Sci., **36**(223), pp. 507–531.
[40] Lemmon, E., Huber, M., and McLinden, M., 2013, "NIST Standard Reference Database 23: Reference Fluid Thermodynamic and Transport Properties-REFPROP, Version 9.1".
[41] Romei, A., Gaetani, P., and Persico, G., 2022, "Computational Fluid-Dynamic Investigation of a Centrifugal Compressor With Inlet Guide Vanes for Supercritical Carbon Dioxide Power Systems," Energy, **255**, p. 124469.
[42] Anderson, J. D., 2003, *Modern Compressible Flow: With Historical Perspective*, McGraw-Hill Education, New York.
[43] Zucrow, M. J., and Hoffman, J. D., 1977, *Gas Dynamics* (Multi-Dimensional Flow; Vol. 2), Wiley.
[44] Zocca, M., Gajoni, P., and Guardone, A., 2023, "NIMOC: A Design and Analysis Tool for Supersonic Nozzles Under Non-Ideal Compressible Flow Conditions," J. Comput. Appl. Math., **429**, p. 115210.
[45] Flock, A. K., and Gülhan, A., 2020, "Design of Converging-Diverging Nozzles With Constant-Radius Centerbody," CEAS Space J., **12**(2), pp. 191–201.
[46] Carnahan, B., 1969, *Applied Numerical Methods*, Wiley, Hoboken, NJ.
[47] Sauer, R., 1947, "General Characteristics of the Flow Through Nozzles at Near Critical Speeds". Technical Report, NACA TM-1147.
[48] Dutton, J. C., and Addy, A. L., 1982, "Transonic Flow in the Throat Region of Annular Supersonic Nozzles," AIAA J., **20**(9), pp. 1236–1243.

[49] Dutton, J. C., and Addy, A. L., 1980, "A Theoretical and Experimental Investigation of Transonic Flow in the Throat Region of Annular Axisymmetric, Supersonic Nozzles". Technical Report, U.S. Army Research Office.
[50] Nederstigt, P., and Pecnik, R., 2023, "Generalised Isentropic Relations in Thermodynamics".
[51] Spinelli, A., Cammi, G., Gallarini, S., Zocca, M., Cozzi, F., Gaetani, P., Dossena, V., and Guardone, A., 2018, "Experimental Evidence of Non-Ideal Compressible Effects in Expanding Flow of a High Molecular Complexity Vapor," Exp. Fluids, **59**(8), p. 126.
[52] Gordon, S., and McBride, B. J., 1994, "Computer Program for Calculation of Complex Chemical Equilibrium Compositions and Applications. Part 1: Analysis". Technical Report, NASA.
[53] Prasad, A., 2004, "Calculation of the Mixed-Out State in Turbomachine Flows," ASME J. Turbomach., **127**(3), pp. 564–572.
[54] Denton, J. D., 1993, "The 1993 IGTI Scholar Lecture: Loss Mechanisms in Turbomachines," ASME J. Turbomach., **115**(4), pp. 621–656.
[55] Moore, J., and Moore, J. G., 1983, "Entropy Production Rates From Viscous Flow Calculations: Part I – A Turbulent Boundary Layer Flow".
[56] Stratford, B. S., and Beavers, G. S., 1961, "The Calculation of the Compressible Turbulent Boundary Layer in an Arbitrary Pressure Gradient - A Correlation of Certain Previous Methods". *Aeronautical Research Council Reports* (3207).
[57] Cebeci, T., and Smith, A., 1974, *Analysis of Turbulent Boundary Layers*, Elsevier, New York.
[58] Pini, M., and De Servi, C., 2020, "Entropy Generation in Laminar Boundary Layers of Non-Ideal Fluid Flows," Non-Ideal Compressible Fluid Dynamics for Propulsion and Power, F. di Mare, A. Spinelli, and M. Pini, eds., Springer International Publishing, pp. 104–117.
[59] Zerobin, S., Peters, A., Bauinger, S., Bhadravati Ramesh, A., Steiner, M., Heitmeir, F., and Göttlich, E., 2018, "Aerodynamic Performance of Turbine Center Frames With Purge Flows–Part I: The Influence of Turbine Purge Flow Rates," ASME J. Turbomach., **140**(6), p. 061009.
[60] Agromayor, R., Müller, B., and Nord, L. O., 2019, "One-Dimensional Annular Diffuser Model for Preliminary Turbomachinery Design".
[61] Brown, W. B., 1947, "Friction Coefficients in a Vaneless Diffuser". Technical Report, Flight Propulsion Research Laboratory, Cleveland, OH.
[62] Shapiro, A. H., 1953, *Dynamic and Thermodynamics of Compressible Fluid Flow*, Vol. I, John Wiley and Sons Inc, Hoboken, NJ.